Talanta 85 (2011) 2166–2174

Contents lists available at ScienceDirect

Talanta

journal homepage: www.elsevier.com/locate/talanta

# Synthesis of polyethylene glycol (PEG) assisted tungsten oxide ($WO_3$) nanoparticles for L-dopa bio-sensing applications

V. Hariharan[a], S. Radhakrishnan[b], M. Parthibavarman[a], R. Dhilipkumar[b], C. Sekar[b,*]

[a] Centre for Nanoscience and Technology, Department of Physics, Periyar University, Salem 636 011, Tamilnadu, India
[b] Department of Bioelectronics and Biosensors, Alagappa University, Karaikudi 630 003, Tamilnadu, India

ARTICLE INFO

*Article history:*
Received 17 May 2011
Received in revised form 16 July 2011
Accepted 18 July 2011
Available online 23 July 2011

*Keywords:*
Tungsten oxide
Microwave irradiation
Poly ethylene glycol
Nanoparticles
L-Dopa
Biosensors

ABSTRACT

Nanocrystalline tungsten oxides ($WO_{3-\delta}$) are currently receiving a lot of attention because of their interesting electrical, magnetic, optical and mechanical properties. In this report, we present the synthesis of PEG assisted tungsten oxide ($WO_3$) nanoparticles by simple household microwave irradiation (2.45 GHz) method. The samples were characterized using powder X-ray diffraction (XRD), thermal analysis (TG/DTA), transmission electron microscopy (TEM), UV–visible diffusion reflectance spectroscopy (UV–VIS-DRS), cyclic voltammetry and electrochemical impedance spectroscopy. Powder XRD results revealed that both the samples prepared with and without surfactant crystallize in the orthorhombic structure corresponding to $WO_3{\cdot}H_2O$ phase. Subsequent annealing under identical conditions (600 °C/air/6 h) led to significantly different products i.e. monoclinic $W_{17}O_{47}$ from surfactant free sample and orthorhombic $WO_3$ from PEG assisted sample. Blue emission was observed through UV–VIS-DRS with blue shift and the band gap energy was estimated as 2.7 and 3.28 eV for PEG assisted as prepared ($WO_3{\cdot}H_2O$) and annealed samples ($WO_3$) respectively. Electrochemical measurements have been performed on all the samples deposited on the surface of glassy carbon (GC) electrode which showed high sensitivity and good selectivity for PEG assisted sample ($WO_3{\cdot}H_2O$) for the direct detection of L-dopa.



## 1. Introduction

The global importance of transition metal oxides in science and technology continuously requires the study and development of suitable synthesis approaches. In particular, metal oxide based semiconducting nanostructures have become a rapidly expanding new field in materials chemistry and physics [1]. Tungsten oxide ($WO_3$), an n type semiconductor, has numerous interesting physical and chemical properties suggesting the potential use of this material in a multitude of applications such as photocatalysis, gas sensors, batteries, photoluminescence, electrochromic, and photo oxidation of water [2]. $WO_{3-\delta}$ nanomaterials can be synthesized by different physical and chemical techniques such as vapor deposition [3], hydrothermal route [4], sol–gel [5], acidification method [6], and electrodeposition method [7]. Recently, surfactant mediated synthesis method plays an important role in nanomaterials research. Huo et al. have developed surfactant templating strategies for the synthesis of oxide based nanomaterials in order to enhance the surface activity of the materials [8]. Poly ethylene glycol (PEG) is used as a surfactant in the synthesis of nanoparticles, because it is an inexpensive organic stabilizer, easily soluble in water, needs no complicated procedure, reactivity at relatively low temperature, etc. Deepa et al. [7] have synthesized nanostructured tungsten oxide films with hybrid structures i.e. nanorods and interconnected nanocrystallites and mesopores from a PEG assisted sol by combining the principles of electrodeposition and templating method. Wolcott et al. [9] investigated the interaction of PEG with $WO_3{\cdot}2H_2O$ and concluded the enhanced behavior for PEG assisted nanoparticles in morphology, crystallanity, and surface activity in addition to charge transport properties.

Nowadays, advances in biosensors based on semiconductor nanostructured metal oxides are of practical and theoretical importance in biological sciences, environmental science and analytical chemistry. L-Dopa, the precursor of dopamine, is an important neurotransmitter which is commonly used for the treatment of neural disorders such as Parkinson's syndrome. *In vitro*, L-dopa is a powerful toxin to the culture of neurons, and may also be toxic *in vivo* according to some animal studies [10]. Therefore, to achieve better curative effect and lower toxicity, the development of a catalytic material for the accurate and specific measurement of L-dopa in different sample matrices is of substantial significance. In order to solve this problem and also considering cost evaluation, great attention have been turned out towards semiconductor metal oxide based nanomaterials on modified glassy carbon electrodes

* Corresponding author. Tel.: +91 9442563637; fax: +91 4565 225202.
*E-mail address:* Sekar2025@gmail.com (C. Sekar).

0039-9140/$ – see front matter © 2011 Elsevier B.V. All rights reserved.
doi:10.1016/j.talanta.2011.07.063

as alternatives. Goyal et al. [11] applied nanoscale $TiO_2$ modified glassy carbon electrode for determination of dopamine. The electrochemical studies illustrated that the detection limit is well below the concentration of dopamine normally present in blood serum and urine. Xia et al. [12] investigated ZnO nanoflowers prepared by mild wet chemical method for dopamine sensing on GC electrode.

In this article, we demonstrate a simple microwave irradiation method to synthesize $WO_{3-\delta}$ nanomaterials with and without using PEG as surfactant for the first time. Compared with conventional synthesis processes, microwave irradiation is quite faster, simpler and more energy efficient. In the microwave irradiation method, time required for synthesis was around 10 min only and the reaction process was also very simple. We shall further discuss electrochemical oxidation of L-dopa on GC modified electrodes.

## 2. Experimental

### 2.1. Materials preparation

The precursor solution was prepared by dissolving 2.49 g of tungstic acid ($H_2WO_4$) in 10 mL of sodium hydroxide (NaOH). This resulted in yellow colored hydrated sodium tungstate solution due to proton exchange protocol process [13]. Subsequently 0.5 g (i.e. 20 wt.% of tungstic acid) of PEG was added to the precursor solution to act as a surfactant and several drops of HCl was introduced into the solution to attain the pH value of 1 in order to enhance the protonation process. HCl can act as a precipitating agent and medium for the product to have desired morphology [14]. About 5 mL double distilled water (i.e. 50 vol.% of precursor solution) was added with the above solution in order to respond to microwave quickly. The final solution was exposed to microwave (2.45 GHz) under optimum power of 180 W for 10 min in air atmosphere. After irradiation a very small amount of surrounding water present in the product was removed by drying at 60 °C in air for 1 h. The above process was repeated without adding PEG under the identical conditions. Both the products resulted in yellow colored powders which were annealed at 600 °C in air for 6 h to attain crystalline anhydrous tungsten oxide. The presence of PEG in the colloid will reduce the nucleation and subsequent growth which controls the size and morphology of $WO_3$ nanoparticles. The overall reaction is presented below.

### 2.2. Materials characterization

Thermal analysis was performed on SDT Q600 V8.3 Build 101. X-ray powder diffraction (XRD) patterns of all the samples were measured on a Bruker AXS D8 advanced diffractometer with monochromatic Cu Kα radiation (λ = 1.5406 Å). TEM images and selected-area electron diffraction (SAED) patterns were recorded on a Technai G20-stwin high resolution electron microscope (HRTEM) using an accelerating voltage of 200 kV. Optical properties were analyzed by UV–visible diffusion reflectance spectroscopy using CARY 5E UV-VIS-NIR spectrophotometer (200–800 nm).

### 2.3. Electrochemical measurements

The electrochemical measurements were performed in a conventional two compartment three electrode cell with mirror polished 0.07 $cm^2$ glassy carbon (GC) as the working electrode, Pt wire as the counter electrode and 3 M KCl Ag/AgCl as the reference electrode using electrochemical workstation (CHI Instruments, USA, Model 6005D). All the measurements were carried out in phosphate buffer solution (PBS, pH 7.2) under nitrogen atmosphere at room temperature. The electrochemical impedance measurements were made by applying ac potential amplitude of 5 mV over the dc potential 200 mV in the frequency range between 100 KHz to 1 Hz. Resulting impedance data are presented in Nyquist plots. Charge transfer rate constant ($R_{CT}$) values were obtained by simulation using Zsimpwin software.

## 3. Results and discussion

### 3.1. Powder XRD analysis

Powder X-ray diffraction data of all the samples were recorded in the 2$\theta$ range from 10° to 80° with Cu Kα radiation (λ = 1.54 Å). XRD pattern of both the as prepared powders (Fig. 1a and b) can be indexed for orthorhombic phase with perovskite-like structure (space group *Pmnb*) in accordance with the JCPDS card no.: 43-0679. It can be noticed that the PEG assisted sample shows sharp and stronger peaks when compared to the surfactant free sample. The occurrence of similar orthorohombic structure is in accordance with the fact that the organic additives only acts as a crystallanity

$$H_2WO_4 + NaOH + HCl + H_2O \rightarrow Na_2WO_4 \cdot 2H_2O + 2HCl \rightarrow WO_3 \cdot H_2O \xrightarrow{600\,^{\circ}C} W_{17}O_{47}$$

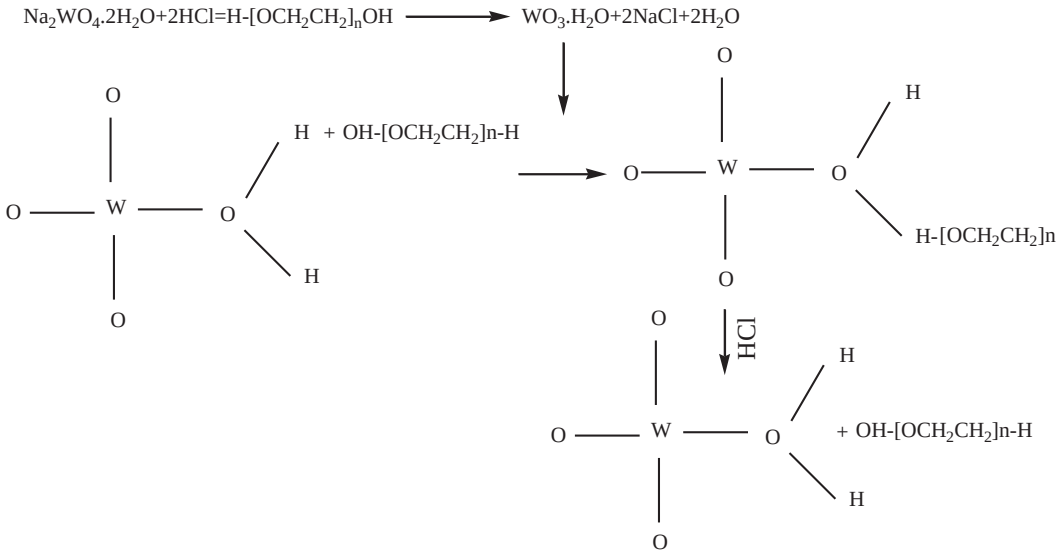

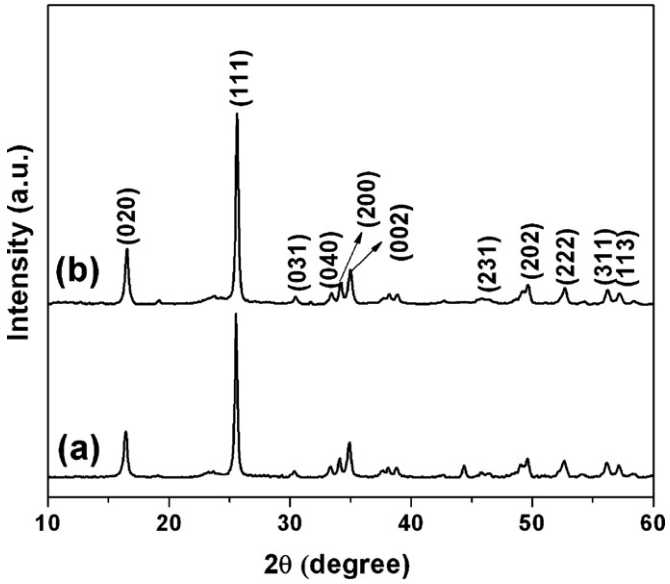


**Fig. 1.** XRD patterns of $WO_3 \cdot H_2O$ synthesized (a) without PEG and (b) with PEG.

controller and never involve in modifying the crystalline structure which is also an important function of PEG-6000 [15].

On the other hand, the presence of PEG-6000 promotes the controlled growth of $WO_3 \cdot H_2O$ crystallites through the formation of hydrogen bonding between hydroxyl group in PEG-6000 and hydrogen ion in $WO_3 \cdot H_2O$ molecule. This reaction results in an intermediate product ($WO_3 \cdot OH–H–[OCH_2CH_2]_n$) and $H_2O$. The highly unstable intermediate product gets reduced to $WO_3 \cdot H_2O$ and PEG-6000 due to acidic conditions prevail in the growth environment (see Section 2.1). The process continues until the crystallite reaches its maximum size [16].

Fig. 2a and b shows the XRD profiles of the samples annealed at 600 °C in air for 6 h. The results confirmed that the surfactant free $WO_3 \cdot H_2O$ is converted into monoclinic phase ($W_{17}O_{47}$) with space group *P2/c* (JCPDS no.: 79-0171) where as PEG assisted $WO_3 \cdot H_2O$ is converted into stoichiometric orthorhombic phase ($WO_3$) with the space group *Pcnb* (JCPDS no.: 89-4480). Thus the oxygen content of

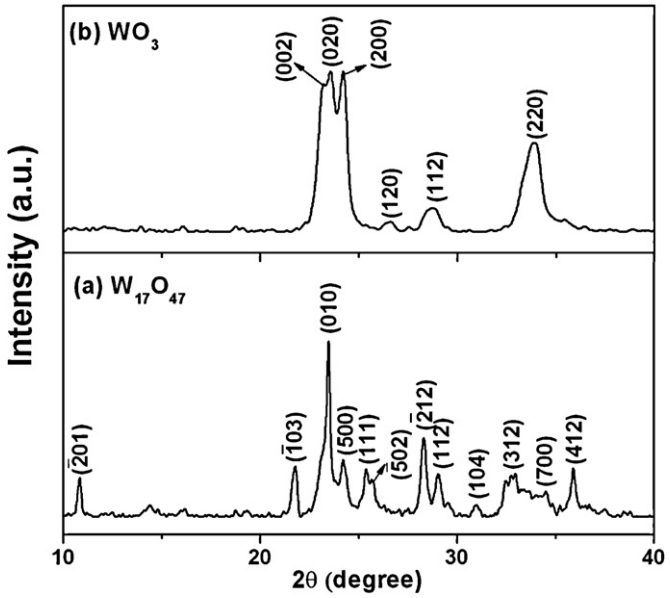


**Fig. 2.** XRD patterns of (a) $W_{17}O_{47}$ (without PEG) and (b) $WO_3$ (with PEG).

**Table 1**
Size of the tungsten oxide crystallites prepared under various conditions.

| Sample | Particle size in nm |
|---|---|
| $WO_3 \cdot H_2O$ | 31.5 |
| $W_{17}O_{47}$ | 32.2 |
| $WO_3 \cdot H_2O$-PEG | 27.7 |
| $WO_3$-PEG | 10.0 |

the end products depends on the nature of the growth environment of the parent compound $WO_3 \cdot H_2O$.

In general, tungsten oxide easily loses oxygen and is represented as $WO_{3-\delta}$. The oxidation state of tungsten in $W_{17}O_{47}$ lies between +4 ($WO_2$) and +6 ($WO_3$). With larger non-stoichiometry the defects preferentially accumulate at so called crystallographic shear planes along (*l*, *m*, o) with the formation of edge-shared $WO_6$ octahedra [17]. In the case of PEG assisted sample, the presence of –OH functional group compensates the amount of oxygen lost during annealing process. Thus the formation of stoichiometric tungsten oxide ($WO_3$) proved the role of PEG in determining the oxygen content of the end product. Recently, we have prepared $WO_3 \cdot H_2O$ using EDTA as surfactant. Subsequent annealing at 600 °C in air for 6 h resulted in oxygen deficient $WO_{2.72}$ phase which has been attributed to the presence of oxygen adsorbing element ($Na^+$ ion) in EDTA [18]. In case of PEG, availability of OH group has promoted the formation of stoichiometric $WO_3$.

Particle size was calculated using Scherrer formula:

$$\Delta x = \frac{0.9\lambda}{\Delta 2\theta \cos\theta}$$

where $2\theta$ is the scattering angle, $\lambda$ is the wavelength of the X-ray used and $\Delta 2\theta$ is full width at half maximum (FWHM) of a Bragg's reflection. The average particle sizes calculated using above equation are shown in Table 1. The random decrease in crystallite size in PEG assisted annealed sample shows the role of PEG on the formation of tungsten oxide.

### 3.2. Thermal analysis (TG/DTA)

Fig. 3a shows the thermo gravimetric (TG) curves recorded on PEG assisted as prepared sample in the temperature range of 30–1200 °C with the heating rate of 20 °C/min in air atmosphere. Initial weight loss (2.9%) up to 166 °C may be due to the removal of physically adsorbed water. Another major weight loss of 10.41%

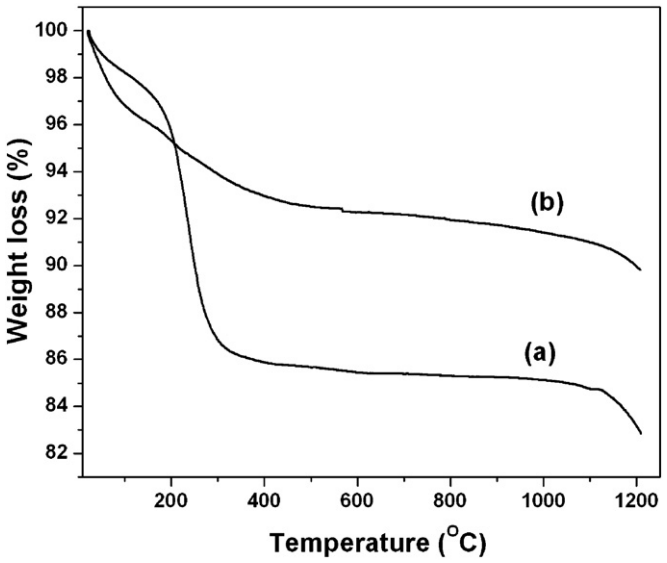


**Fig. 3.** TG curves of $WO_3 \cdot H_2O$ (a) with PEG and (b) without PEG.

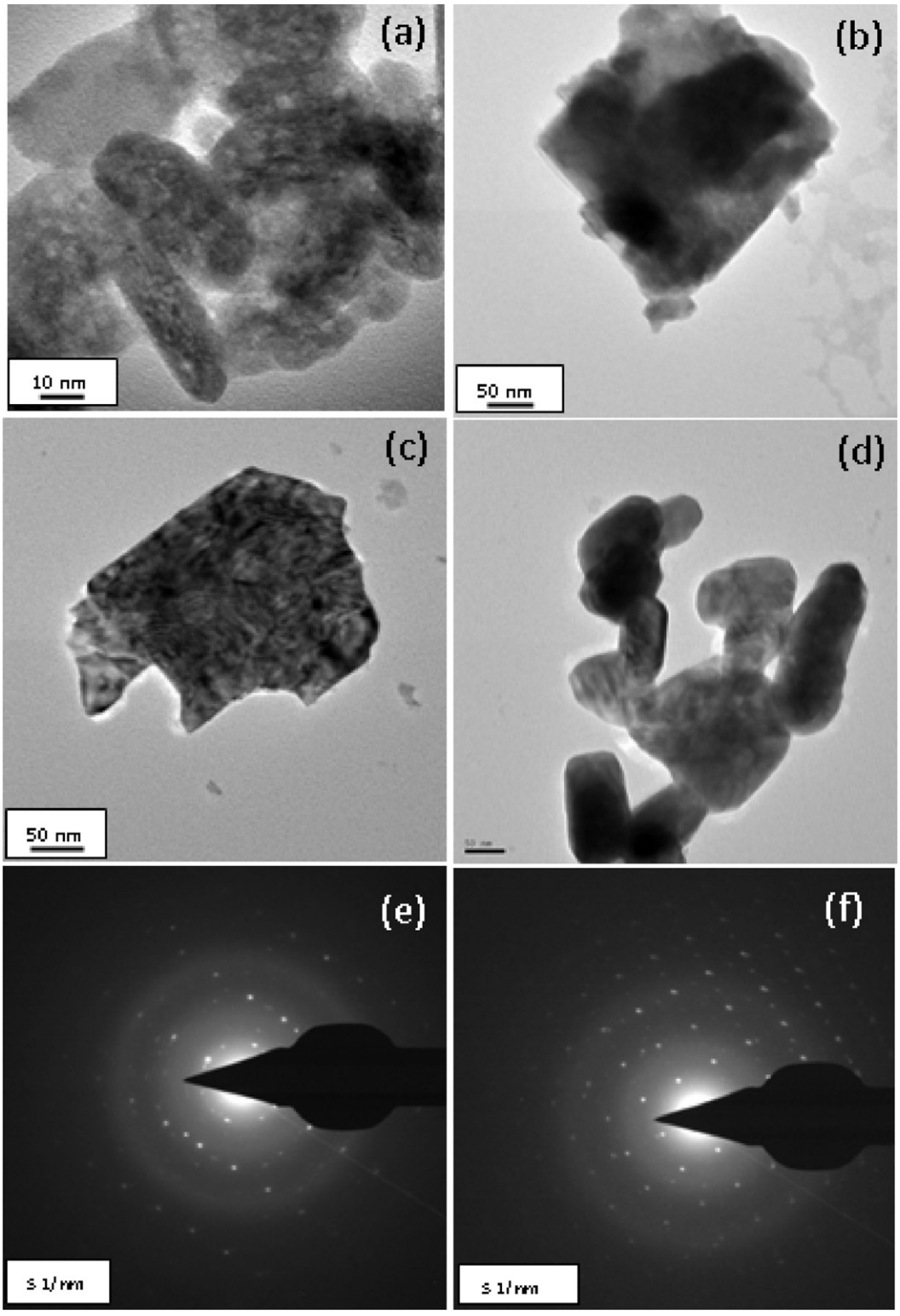


**Fig. 4.** TEM images of (a) $WO_3 \cdot H_2O$ (without PEG), (b) $W_{17}O_{47}$, (c) $WO_3 \cdot H_2O$ (with PEG) and (d) $WO_3$-PEG. SAED patterns of $WO_3 \cdot H_2O$-without PEG (e) and $WO_3 \cdot H_2O$-PEG (f).

was observed in the temperature range between 167 and 311 °C which could be attributed to the loss of some chemically bonded water and organic species released during the crystallization process [19]. There has been no significant change in mass with further heating up to 1200 °C which confirms the phase stability of $WO_3$ over the wide temperature range between 300 and 1200 °C in air atmosphere. In the case of surfactant free $WO_3 \cdot H_2O$ (Fig. 3b) the total weight loss was found to be only 7%. This is much less than that of the sample (13.33%) $WO_3 \cdot H_2O$ prepared using PEG which clearly indicates role of PEG in fixing the oxygen content and stability of the end product.

### 3.3. TEM analysis

Fig. 4a and b shows the TEM micrographs of surfactant free as prepared ($WO_3 \cdot H_2O$) and annealed ($W_{17}O_{47}$) samples. The as

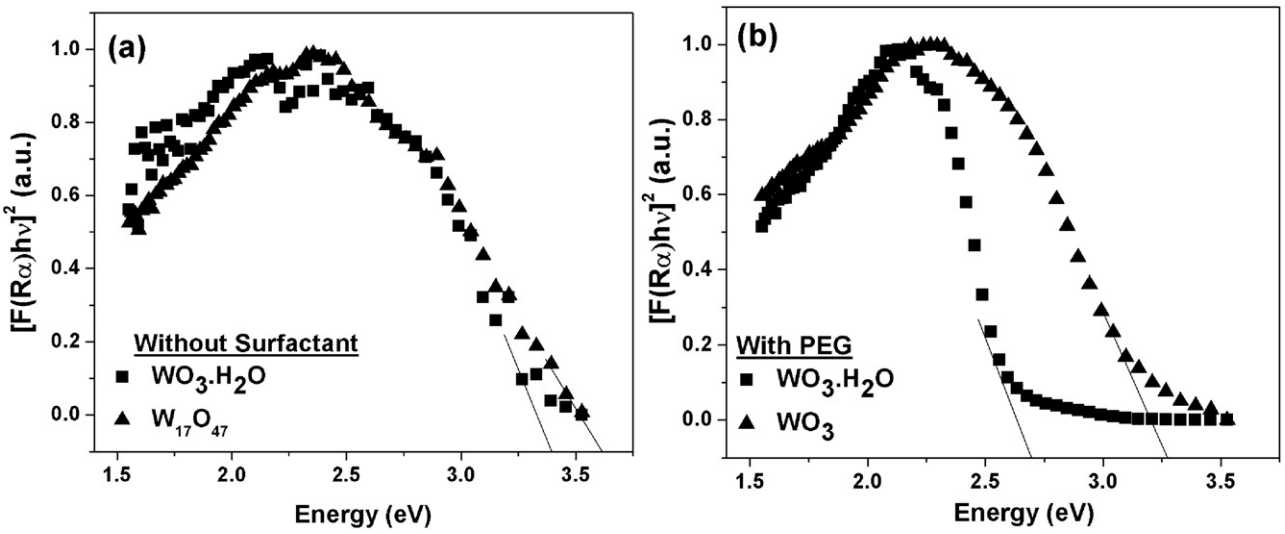


**Fig. 5.** K–M model of UV–VIS-DRS spectra of tungsten oxides synthesized (a) without PEG and (b) with PEG.

prepared sample consisted of nanosized tablets of different dimensions (Fig. 4a). Upon annealing at 600 °C in air for 6 h, these tiny particles aggregated and resulted in platelet-like morphology (Fig. 4b). In the case of PEG assisted synthesis, the as prepared samples ($WO_3 \cdot H_2O$) consisted of sheet like structure (Fig. 4c) with the dimensions of the order of 230 nm in length and 270 nm in width. Subsequent annealing resulted in stoichiometric $WO_3$ with well dispersed confined elongated sphere like morphology (Fig. 4d) with dimensions of the order of 70–110 nm in length and 40–80 nm in width. The occurrence of a very uniform electron diffraction spots (see inset of Fig. 4a) in the as prepared surfactant free $WO_3 \cdot H_2O$ confirms its single crystalline nature. Interestingly, the PEG assisted sample (see inset of Fig. 4c) has high crystallanity when compared to the surfactant free sample. The results suggest that the controlled growth of the tungsten oxide nanoparticles in the presence of PEG leads to high crystallanity in agreement with the powder XRD data.

### 3.4. UV–visible diffusion reflectance analysis

The diffuse reflectance spectroscopy was performed on all the samples. The absorption from 550 to 450 nm towards lower wavelengths in the entire spectrum (blue shift) corresponds to the absorption edge of the solids and it is due to the transition from $O^{2-}$ to $M^{n+}$ [mainly transfer of 2p orbital of the oxygen anions to 5d orbital of the tungsten cation] which indicates the quantum confinement effect [20].

The band gap energies calculated using Kubelka–Munk (K–M) model are described below. The K–M model at any wavelength is given by

$$\frac{K}{S} = \frac{(1 - R_\infty)^2}{2R_\infty} = F(R_\infty)$$

where $F(R_\alpha)$, the so called remission or Kubelka–Munk function is defined as

$$R_\infty = \frac{R_{\text{sample}}}{R_{\text{standard}}}$$

A graph is plotted between $[F(R_\alpha)h\nu]^2$ vs. $h\nu$ and the intercept value is the band gap energy $E_g$ of the individual sample [21]. The band gap energies were thus estimated as 2.7 eV for $WO_3 \cdot H_2O$ prepared with PEG and 3.28 eV for the same sample after annealing at 600 °C ($WO_3$) respectively (Fig. 5a). Similar procedure was followed to calculate the band gap energies for $WO_3 \cdot H_2O$ and $W_{17}O_{47}$ prepared without PEG and the values were found to be 3.40 and 3.55 eV (Fig. 5b) respectively. The increase in band gap energy of the surfactant free samples is mainly due to increase in oxygen vacancies. This indicates that the PEG assisted samples have more optical conductivity than the surfactant free samples.

## 4. Fabrication of glassy carbon electrode modified with tungsten oxide nanoparticles

The bare glassy carbon electrode was polished to a mirror like surface with 0.05 μm alumina powder and sonicated in water for 5 min. One hundred milligrams of $WO_3$ nanoparticles was dispersed in 10 mL anhydrous alcohol under ultrasonication for 30 min, then 10 μL of alcoholic dispersed $WO_3$ was dropped onto the glassy carbon surfaces and air dried at room temperature.

### 4.1. Electrochemical impedance measurements

The charge transport process in $WO_3$ modified electrode has been studied by monitoring charge transfer resistance ($R_{CT}$) at the

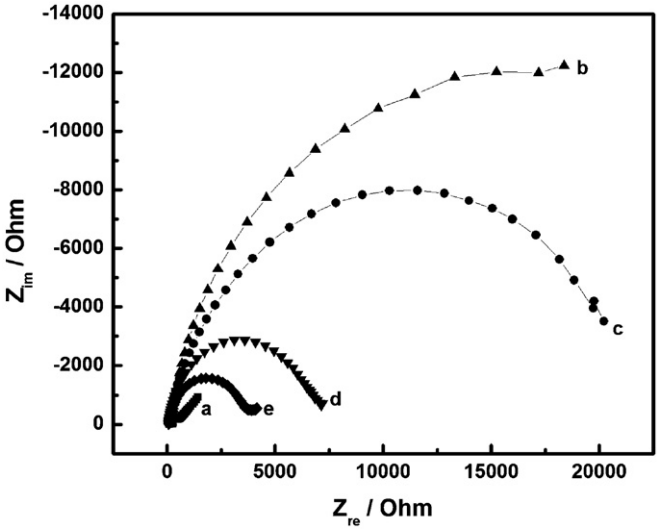


**Fig. 6.** Electrochemical impedance spectra of (a) bare GC, (b) $WO_3 \cdot H_2O$, (c) $W_{17}O_{47}$, (d) $WO_3 \cdot H_2O$-PEG, and (e) $WO_3$-PEG.

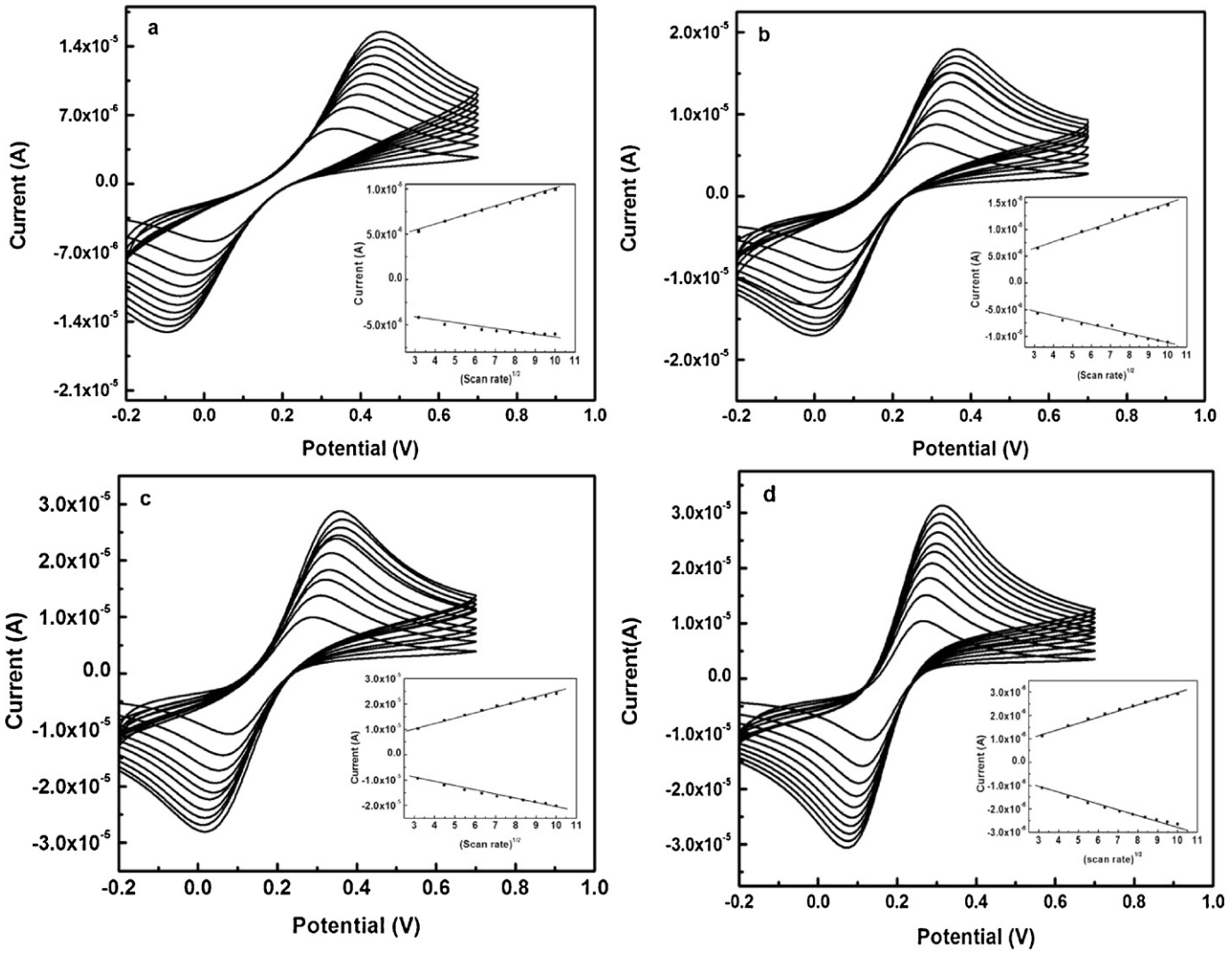


**Fig. 7.** Cyclic voltammograms recorded at 10–100 mV $s^{-1}$ for (a) $WO_3{\cdot}H_2O$, (b) $W_{17}O_{47}$, (c) $WO_3{\cdot}H_2O$-PEG, and (d) $WO_3$-PEG modified electrodes in phosphate buffer solution. (10 mM; pH 7.2) containing $[Fe(CN)_6]^{3-/4-}$ (1 mM). Inset: plots of peak currents versus square root of scan rate.

electrode–electrolyte interface (Fig. 6). The value of electron transfer resistance depends on the dielectric and insulating features at the electrode/electrolyte interface. The $R_{CT}$ value for bare GC, $WO_3{\cdot}H_2O$, $W_{17}O_{47}$, $WO_3{\cdot}H_2O$-PEG and $WO_3$-PEG modified electrodes have been estimated as 383, 24,810, 15,480, 6481 and 3505 Ω, respectively. The $R_{CT}$ value of $W_{17}O_{47}$ (annealed) is higher than that of the PEG assisted samples. This could be attributed to the oxygen deficiency in $W_{17}O_{47}$. The lower $R_{CT}$ is obtained for $WO_3$-PEG sample. These results are in agreement with the band gap energy value ($E_g$) obtained from UV–VIS-DRS measurements.

### 4.2. Cyclic voltammetric studies

Fig. 7a–d shows various cyclic voltammograms recorded at different scan rates (10–100 mV $s^{-1}$) for $WO_3{\cdot}H_2O$, $W_{17}O_{47}$, $WO_3{\cdot}H_2O$-PEG, $WO_3$-PEG modified electrodes in PBS (10 mM; pH 7.2) containing $[Fe(CN)_6]^{3-/4-}$ (1 mM). It can be seen that the anodic potential (Fig. 7a–d) shifts towards positive side and the cathodic peak potential shifts in the reverse direction. Besides this, the redox peak currents are proportional to the square root of scan rate (inset of Fig. 7) which indicates diffusion electron-transfer process. It can be noticed (Fig. 7a and b) that the redox potential of $WO_3{\cdot}H_2O$ and $W_{17}O_{47}$ modified electrodes shifts towards the higher side than that of $WO_3$-PEG modified electrode. These observations suggest that the electron transfer rate of the PEG assisted samples is higher than that of surfactant free samples.

The surface concentration of the $WO_3$ film can be estimated from the plot of current versus potential (CV) using Brown–Anson model that is based on the following equation:

$$Ip = \frac{n^2F^2I^*AV}{4RT}$$

where $n$ is the number of electrons transferred, $F$ is the Faraday constant (96,485 C $mol^{-1}$), $I^*$ is the surface concentration (mol $cm^{-2}$). $A$ is the surface area of the electrode (0.07 $cm^2$), $V$ is the scan rate (50 mV $s^{-1}$), $R$ is the gas constant (8.314 J $mol^{-1}$ $K^{-1}$) and $T$ is the absolute temperature (298 K). The value of the surface concentration of the $WO_3{\cdot}H_2O$, $W_{17}O_{47}$, $WO_3{\cdot}H_2O$-PEG and $WO_3$-PEG modified electrodes has been estimated to be $3.078 \times 10^{-9}$, $3.592 \times 10^{-9}$, $5.8671 \times 10^{-9}$ and $5.6025 \times 10^{-9}$ mol $cm^{-2}$ respectively. The difference in surface concentrations on GC electrode clearly indicate that the PEG mediated $WO_3{\cdot}H_2O$ film has high density when compared to surfactant free samples.

Fig. 8 shows cyclic voltammograms recorded at 50 mV $s^{-1}$ for (a) bare GC, (b) $WO_3{\cdot}H_2O$ (c) $W_{17}O_{47}$, (d) $WO_3{\cdot}H_2O$-PEG and (e) $WO_3$-PEG modified electrodes in PBS (10 mM; pH 7.2)

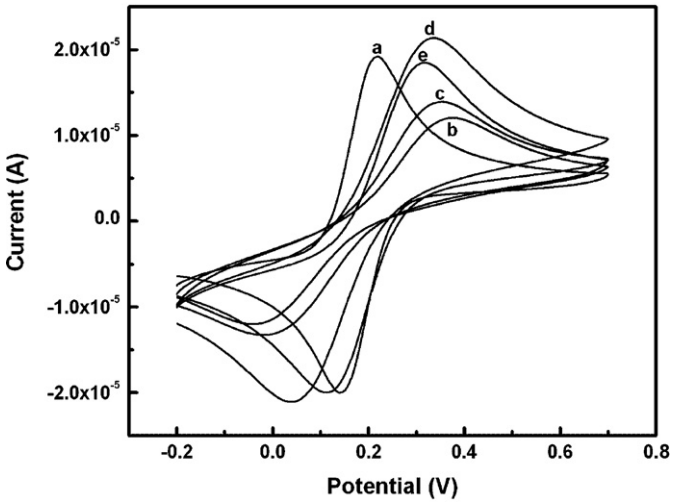


**Fig. 8.** Cyclic voltammograms recorded at 50 mV $s^{-1}$ for (a) bare GC, (b) $WO_3{\cdot}H_2O$, (c) $W_{17}O_{47}$, (d) $WO_3{\cdot}H_2O$-PEG, and (e) $WO_3$-PEG modified electrodes in phosphate buffer (10 mM; pH 7.2) containing $[Fe(CN)_6]^{3-/4-}$ (1 mM).

containing $[Fe(CN)_6]^{3-/4-}$ (1 mM). The peak separation of 73 mV, 373 mV, 325 mV, 269 mV and 187 mV were observed for the bare GC, $WO_3{\cdot}H_2O$, $W_{17}O_{47}$, $WO_3{\cdot}H_2O$-PEG and $WO_3$-PEG modified electrodes respectively. This observation confirmed that the electron transfer rate of the PEG assisted $WO_3$ is higher when compared to that of the surfactant free samples.

### 4.3. Electrochemical oxidation of L-dopa

We have made an attempt to use nano tungsten oxide modified glassy carbon electrodes for the sensing of L-dopa. The PEG assisted $WO_3{\cdot}H_2O$ showed higher electro catalytic activity towards the detection of L-dopa at physiological pH 7.2. Fig. 9(A) depicts the CVs of 1 mM L-dopa at the bare and different tungsten oxide modified GC electrodes in 10 mM phosphate buffer solution (pH 7.2). The oxidation peak current was observed for bare GC (curve *a*), $WO_3{\cdot}H_2O$ (curve *b*), $W_{17}O_{47}$ (curve *c*), $WO_3{\cdot}H_2O$-PEG (curve *d*) and (e) $WO_3$-PEG (curve *e*) as $2.84\times10^{-5}$ A, $2.36\times10^{-5}$ A, $2.64\times10^{-5}$ A, $4.64\times10^{-5}$ A and $3.96\times10^{-5}$ A respectively. A nearly 2-fold increase in oxidation current was obtained for L-dopa at the $WO_3{\cdot}H_2O$-PEG modified electrode when compared to the bare GC electrode. Hence, we have chosen $WO_3{\cdot}H_2O$-PEG modified electrode for further investigations. The effect of scan rate on the oxidation of L-dopa is shown in Fig. 9(B). It can be noted that the L-dopa peak current increases with the increase in scan rate. A good linearity between the anodic peak current and the square root of the scan rate with a correlation coefficient of $R = 0.98$ was obtained within the range of 10–80 mV $s^{-1}$. This indicated that the reaction of electrode with L-dopa was through diffusion control process.

Fig. 10(A) shows the linear sweep voltammograms (LSVs) obtained for L-dopa in the concentration range of 0–100 μM at the $WO_3{\cdot}H_2O$-PEG modified electrode. The oxidation current of L-dopa got enhanced with the increase in L-dopa concentration (each step with the increment of 5 μM). The oxidation current has a linear relationship with concentration of L-dopa with a correlation coefficient of 0.9980 (data not shown). Furthermore, the amperometric study was performed to examine the sensitivity of the $WO_3{\cdot}H_2O$-PEG modified electrode towards the detection of L-dopa. Fig. 10(B) depicts the amperometric *i*–*t* curve for L-dopa at the $WO_3{\cdot}H_2O$-PEG modified electrode in a homogeneously stirred 10 mM PB solution at an applied potential of +0.5 V. The modified electrode showed an initial response due to 100 nM L-dopa and on adding the same quantity of L-dopa in each step with a sample interval of 50 s, the current response linearly increased, and a steady state current response was attained within 4 s. The amperometric current linearly increased when the concentration of L-dopa was increased from $1.0\times10^{-7}$ to $1.0\times10^{-6}$ M at the $WO_3{\cdot}H_2O$-PEG modified electrode with a correlation coefficient of 0.993. The detection limit was found to be 120 nM (inset of Fig. 10(B)). This value is very much comparable to the literature values (Table 2).

The preparation of electrode employed in the present study is very simple when compared to the reported tedious procedures. Further, the $WO_3{\cdot}H_2O$-PEG electrode was found to be stable with good selectivity and sensitivity. We have estimated the current response of 100 nM L-dopa to be 45.0 nA from Fig. 10(B), which gave the sensitivity of 0.45 nA for 1 nM.

### 4.4. Selective determination of L-dopa in the presence of interfering compounds using the $WO_3$-PEG modified electrode

We have investigated the possible interfering compounds for determination of L-dopa (Fig. 11). The oxidation peak current did not change, even in the presence of 100-fold excess of

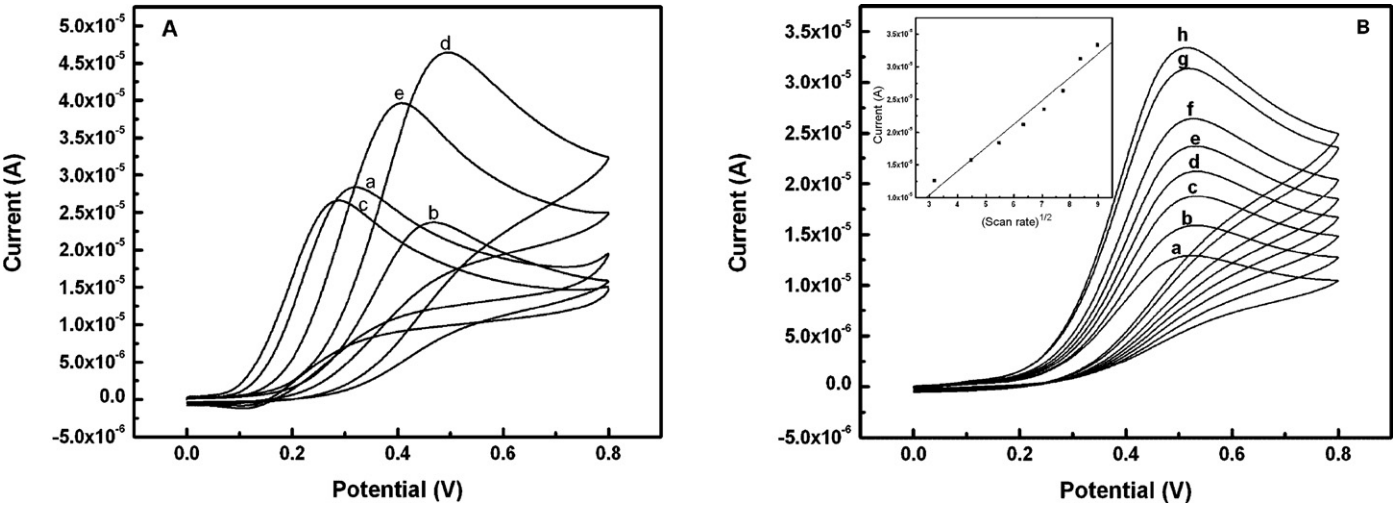


**Fig. 9.** (A) Cyclic voltammograms recorded at 100 mV $s^{-1}$ for (a) bare GC, (b) $WO_3{\cdot}H_2O$, (c) $W_{17}O_{47}$, (d) $WO_3{\cdot}H_2O$-PEG, and (e) $WO_3$-PEG modified electrodes in phosphate buffer (10 mM; pH 7.2) containing 1 mM L-dopa. (B) CVs obtained for 1 mM L-dopa at the $WO_3{\cdot}H_2O$-PEG modified GC electrode in 10 mM PBS at different scan rates: (a) 10, (b) 20, (c) 30, (d) 40, (e) 50, (f) 60, (g) 70 and (h) 80 mV $s^{-1}$. Inset: oxidation current vs. square root of scan rate.

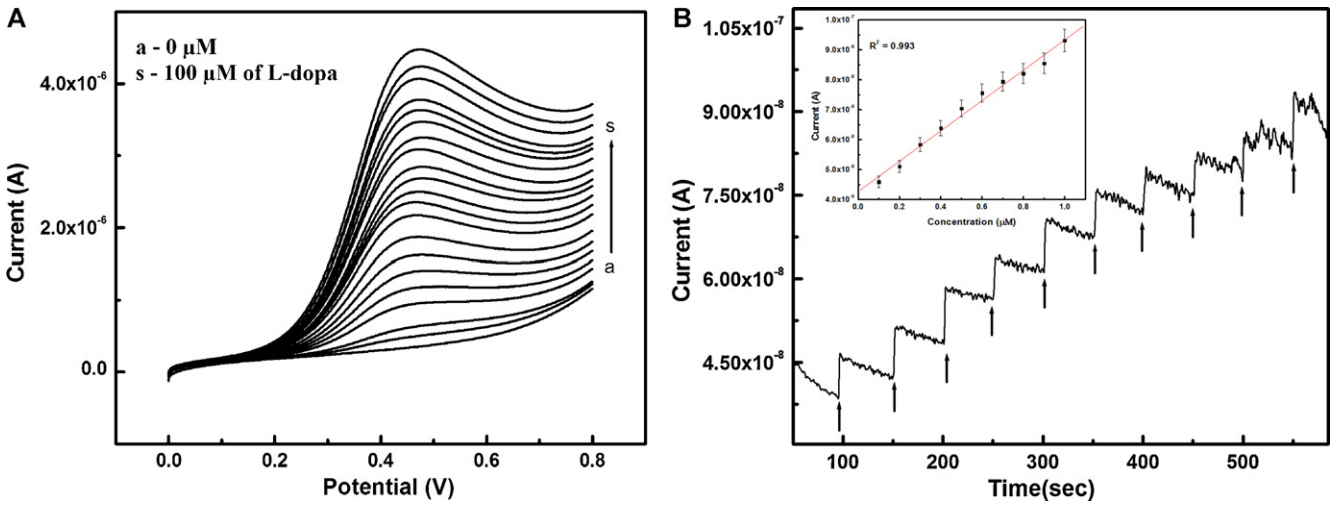


**Fig. 10.** (A) LSVs obtained for L-dopa in the concentration ranging from 0 to 100 μM. L-Dopa was added in steps of 5 μM each at the $WO_3{\cdot}H_2O$-PEG modified electrode in 10 mM PB solution. (B) Amperometric *i–t* curve for the determination of L-dopa at the $WO_3{\cdot}H_2O$-PEG modified electrode in 10 mM PB solution. Each addition increases the concentration of 100 nM at regular interval of 50 s (arrows indicate the L-dopa injection). $E_{app}$ = +0.50 V. Inset shows the calibration plot. The noise is due to stirring the analyte solution.

**Table 2**
Performance of the $WO_3{\cdot}H_2O$-based L-dopa sensor in comparison with reported sensors.

| Electrode | pH | Linear range (M) | Detection limit (M) | Ref. |
|---|---|---|---|---|
| AuNP-CNT-PGE | 7.0 | $0.1\times10^{-6}$–$1.5\times10^{-8}$ | $50\times10^{-9}$ | [22] |
| p-NiII TAPc-GCE | 4.0 | $1.0\times10^{-7}$–$7.0\times10^{-7}$ | $10\times10^{-8}$ | [23] |
| GNP-MEA-NIHCF | 7.0 | $8.2\times10^{-7}$–$2.5\times10^{-3}$ | $53\times10^{-8}$ | [24] |
| MWCNT-PPy-GCE | 7.0 | $1.0\times10^{-6}$–$10\times10^{-5}$ | $10\times10^{-7}$ | [25] |
| Disposable electrode | 3.0 | $9.9\times10^{-5}$–$1.2\times10^{-3}$ | $68\times10^{-6}$ | [26] |
| Polycarbazole electrode | 7.0 | $1.0\times10^{-3}$–$1.0\times10^{-2}$ | – | [27] |
| Oxavandium salen thin film electrode | 6.0 | $1.0\times10^{-6}$–$1.0\times10^{-4}$ | $80\times10^{-8}$ | [28] |
| PEDOT-SWNT | 7.0 | $2.0\times10^{-5}$–$1.0\times10^{-1}$ | $10\times10^{-8}$ | [29] |
| $WO_3{\cdot}H_2O$-GCE | 7.2 | $1.0\times10^{-7}$–$1.0\times10^{-6}$ | $12\times10^{-8}$ | This work |

physiological interfering compounds such as glucose, uric acid and urea. These physiological interfering compounds got oxidized above the applied potential ($E_{app}$) of 0.5 V at the $WO_3{\cdot}H_2O$-PEG modified electrode. Thus, $WO_3{\cdot}H_2O$-PEG modified film was highly selective towards L-dopa from the aforementioned interfering compounds.

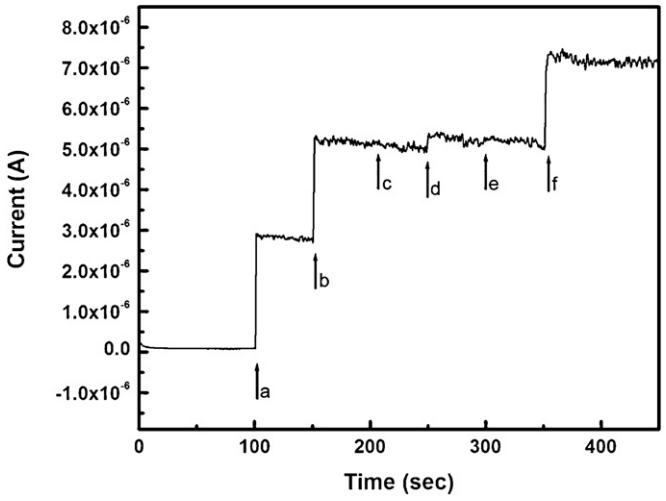


**Fig. 11.** Amperometric *i–t* curve for the addition of 0.5 μM of L-dopa curves (*a* and *b*) and 0.5 mM of uric acid, glucose and urea curves (*c–e*) and final addition of 0.5 μM of L-dopa (*f*) at $WO_3{\cdot}H_2O$-PEG modified electrode in phosphate buffer solution (pH 7.2). $E_{app}$ = +0.50 V.

## 5. Conclusions

We have successfully synthesized tungsten oxide nanoparticles by adopting a novel microwave irradiation method using PEG-6000 as surface modulator. The powder XRD investigations confirmed that the surfactant free $WO_3{\cdot}H_2O$ yielded non stoichiometric $W_{17}O_{47}$ and PEG assisted $WO_3{\cdot}H_2O$ produced $WO_3$ upon heating under identical conditions (600 °C/air/6 h). The results confirmed the significant role of PEG in fixing the oxygen content of the end products. TEM observation revealed that the sample $WO_3$-PEG consisted of well separated elongated spheres composed of nanoparticles. UV–VIS-DRS analysis indicated that the optical conductivity of surfactant free samples is lower than that of the PEG assisted samples. Series of electrochemical experiments were carried out incorporating the different types of tungsten oxide nanoparticles for L-dopa sensing application on a GC electrode. The results showed that the PEG assisted samples had high sensitivity and good selectivity when compared to that of surfactant free samples.

## Acknowledgments

The authors thank Drs. V. Dharuman and J. Wilson, Department of Bioelectronics and Biosensors, Alagappa University for extending their UGC, Govt. of India funded electrochemical workstation (CHI model 6005D, USA) to carryout electrochemical measurements. Use of HRTEM facility of Unit on Nanoscience and Nanotechnology Initiative at IIT Delhi (Project No. SR/S5/NM-22/2004) of the

Department of Science and Technology, Government of India is gratefully acknowledged.

## References

[1] E. Lassner, W.D. Schubert, Tungsten – Properties Chemistry Technology of the Element Alloys and Chemical Compounds, first ed., Springer, New York, 1999.
[2] P.A. Cox, Transition Metal Oxides, Clarendon Press, Oxford, 1995.
[3] S. Bruyère, V. Potin, M. Gillet, B. Domenichini, S. Bourgeois, Thin Solid Films 517 (2009) 6565–6568.
[4] R. Huirache-Acuña, F. Paraguay-Delgado, M.A. Albiterd, J. Lara-Romerod, R. Martínez-Sánchez, Mater. Charact. 60 (2009) 932–937.
[5] W. Wang, Y. Pang, S.N.B. Hodgson, Micropor. Mesopor. Mater. 121 (2009) 121–128.
[6] T. Kida, A. Nishiyama, M. Yuasa, K. Shimanoe, N. Yamazoe, Sens. Actuators B 135 (2009) 568–574.
[7] M. Deepa, M. Kar, D.P. Singh, A.K. Srivastava, S. Ahmad, Solar Energy Mater. Solar Cells 92 (2008) 170–178.
[8] Q. Huo, D.I. Margolese, U. Ciesla, D.G. Demuth, P. Feng, T.E. Gier, P. Sieger, A. Firousi, B.F. Chmelka, F. Sch¨uth, G.D. Stucky, Chem. Mater. 6 (1994) 1176–1191.
[9] A. Wolcott, T.R. Kuykendall, W. Chen, S. Chen, J.Z. Zhang, J. Phys. Chem. B 110 (2006) 25288–25296.
[10] F. Kong, H. Liu, J. Dong, W. Qian, Biosens. Bioelectron. 26 (2011) 1902–1907.
[11] R.N. Goyal, D. Kaur, A.K. Panday, Open Chem. Biomed. Methods J. 3 (2010) 115–122.
[12] C. Xia, W. Ning, W. Long, C. Lin, Sens. Actuators B 147 (2010) 629–634.
[13] C. Santato, M. Ulmann, J. Augustynski, J. Phys. Chem. B 105 (2001) 936–940.
[14] T. Jesionowski, Powder Technol. 127 (2002) 56–65.
[15] J.K. Kim, K. Shin, S.M. Cho, T. Lee, J.H. Park, Energy Environ. Sci. 4 (2011) 1465–1470.
[16] Y. Zhou, H. Yao, Q. Zhang, J. Gong, S. Liu, S. Yu, Inorg. Chem. 48 (2009) 1082–1090.
[17] J. Dattatray, V. Late Ranjit, K.C.S. Rout, A. Mahendra, S.M. Dilip, S. Joag, Appl. Phys. A 98 (2010) 751–756.
[18] V. Hariharan, M. Parthibavarman, C. Sekar, J. Alloys Compd. 509 (2011) 4788–4792.
[19] W. Cheng, E. Baudrin, B. Dunn, J.I. Zinc, J. Mater. Chem. 10 (2000) 1–18.
[20] C. Martin, I. Martin, V. Rives, G. Solana, V. Loddo, L. Palmisano, A. Sclafani, J. Mater. Sci. 32 (1997) 6039–6047.
[21] A. Escobedo Morales, E. Sĩanchez Mora, U. Pal, Rev. Mex. Fis. 53 (2006) 18–22.
[22] H. Guangzhi, C. Long, G. Yong, W. Xiaolai, S. Shijun, Electrochem. Acta 55 (2010) 4711–4716.
[23] A. Sivanesan, S. Abraham John, Biosens. Bioelectron. 23 (2007) 708–713.
[24] P. Prabhu, R. Suresh Babu, S. Sriman Narayanan, Sens. Actuators B 156 (2011) 606–614.
[25] S. Shahrokhian, E. Asadian, J. Electroanal. Chem. 636 (2009) 40–46.
[26] M.F. Bergamini, A.L. Santos, N.R. Stradiotto, M.V.B. Zanoni, J. Pharm. Biomed. Anal. 39 (2005) 54–59.
[27] R.B. Kawde, N.B. Laxmeshwar, K.S.V. Santhanam, Sens. Actuators B 23 (1995) 35–39.
[28] M.F.S. Teixeira, L.H. Marcolino-Junior, O. Fatibello-Filho, E.R. Dockal, M.F. Bergamini, Sens. Actuators B 122 (2007) 549–555.
[29] J. Mathiyarasu, L. Nyholm, Electroanalysis 22 (2010) 449–454.